Tuning interfacial spin filters from metallic to resistive within a single organic semiconductor family

Jingying Wang, Andrew Deloach, Wei Jiang, Christopher M. Papa, Mykhaylo Myahkostupov, Felix N. Castellano, Feng Liu, and Daniel B. Dougherty

Phys. Rev. B **95**, 241410 — Published 30 June 2017

DOI: 10.1103/PhysRevB.95.241410

Tuning Interfacial Spin Filters from Metallic to Resistive within a Single Organic Semiconductor Family

Jingying Wang[1], Andrew Deloach[1], Wei Jiang[2], Christopher M. Papa,[3] Mykhaylo Myahkostupov[3], Felix N. Castellano[3], Feng Liu[2], Daniel B. Dougherty[1]

[1] Department of Physics, North Carolina State University, Raleigh, North Carolina 27695-8202, USA

[2] Department of Material Science & Engineering, University of Utah, Salt Lake City, Utah, 84112, USA

[3] Department of Chemistry, North Carolina State University, Raleigh, North Carolina 27695-8204, USA

A metallic spin filter is observed at the interface between Alq_3 adsorbates and a Cr(001) surface. It can be changed to a resistive (i.e. gapped) filter by substituting Cr ions to make Crq_3 adsorbates. Spin polarized scanning tunneling microscopy and spectroscopy shows these spin dependent electronic structure changes with single molecule resolution. Density functional theory calculations highlight the structural and electronic differences at the interfaces. For Alq_3, a charge transfer interaction with the substrate leads to a metallic spin filter. For Crq_3, direct covalent interactions mix molecular orbitals with the substrate surface state to make two well-separated interfacial hybrid orbitals.

PACS:73.20.-r, 68.37.Ef, 75.70.Rf, 74.20.Fg

*Corresponding Author:dbdoughe@ncsu.edu

Organic semiconductor materials are of interest for spintronics since their magnetic properties can be tuned by well-known synthetic chemistry.[1, 2] As with all semiconductors, organic semiconductor-metal interfaces are decisive for spin injection.[3-5] Rather than designing a perfect Ohmic contact as for a traditional electronic device, it is necessary to create a spin-dependent interfacial resistance[6] such as a tunnel barrier,[7] Schottky barrier,[8] or magnetic interface state.[4] This kind of hybrid interface state has been invoked to explain the unexpectedly large 300% tunneling magnetoresistance (TMR) values observed for nanopore devices with *tris*-(8-hydroxyquinolate)-aluminum (Alq_3) spacer layers.[3] The large TMR value requires that the effective Fermi level spin polarization at the interface is significantly increased by interaction with the molecule and thus acts as a "spin filter". Here we report a specific qualitative mechanism for such spin filtering at a model metal-Alq_3 interface using spin-resolved electronic structure observations and first principles computations. We also show the extreme sensitivity of this interfacial effect to small molecular changes by comparing with a variant of Alq_3, Crq_3. The later paramagnetic variant of Alq_3 realizes a resistive spin filter defined by previously unknown[9] bonding and antibonding interface states with opposite spin polarization.

Interfacial spin filtering based on band symmetry has been very successful in tunneling-based spintronics.[10] It leads to dramatic orbital symmetry filtering at transition metal-MgO interfaces and correspondingly large TMR.[11] Alternately, magnetic semiconductors with exchange split bands provide the canonical example of a spin filter where the spin-dependent injection barriers into the bands allow one spin to pass exponentially more efficiently than the other.[10] In the realm of organic spintronics, the possibility to use molecular design to control interfacial spin filtering is a major opportunity that is independent of ongoing debate[12, 13] about the nature of spin transport within this materials class.

Interfacial spin filters can be categorized from a spectroscopic perspective as either metallic or resistive depending on the whether they exhibit a spin polarized density of states at the

Fermi level or not.[4] For organic materials, experimental evidence has been obtained for metallic spin filters in phthalocyanines on iron and cobalt substrates[14-17] and for other molecules such as simple hydrocarbons in computational work.[18] Reports of resistive spin filters can be found for metal phthalocyanines,[19-21] spin crossover compounds,[22] hydrocarbons,[23] transition metal radicals,[24] and fullerenes[25] on various substrates.

Here we focus single molecule spin polarized STM studies on the most commonly used organic semiconductor in organic spintronic devices, the Alq_3 molecule adsorbed on the Cr(001) surface which has a surface state analogous to those involved in symmetry filtering in oxides.[1, 26] Devices based on Alq_3 films with different magnetic electrodes and geometries have shown large magnetoresistive effects that have spurred consideration of hybrid interface state formation.[26-29] Observations of spin polarized metal-molecule hybridization in Alq_3 have been made using of X-ray magnetic circular dichroism (XMCD) at the N K-edge for Alq_3/Fe(001) that associates the magnetic effects with unoccupied molecular states.[30] In addition, long-lived hybrid states with a spin dependent lifetime have been identified by spin polarized photoemission for Alq_3 films on a cobalt electrode[31] and recently attributed to second layer "dynamic spin filter" effects.[32]

We applied spin-polarized scanning tunneling microscopy/spectroscopy (SP-STM/STS, see Supplemental Materials[33])[34] to characterize hybrid interface states for Alq_3 and the analogous Crq_3 molecules (synthesized by a known method[33, 35, 36]) adsorbed on the Cr(001) surface. We use bulk Cr tips known to have a canted magnetic moment with dominant in-plane sensitivity.[37] Functional magnetic tips were created with high yield by fracturing and then etching polycrystalline Cr chunk and then annealing with electron bombardment in ultrahigh vacuum. The comparison between these molecules demonstrates the extreme sensitivity of interface state formation to molecular electronic structure. In particular, Crq_3 is a paramagnetic (S=3/2) analog of Alq_3 and exhibits slightly different molecular orbitals from Alq_3 as shown by DFT calculations (Supplemental Figure S1[33]).[38, 39] The lowest unoccupied molecular orbital (LUMO) of Crq_3

involves some mixing of the *d* orbitals of central metal atom with the π orbitals on the quinolate ligand. By contrast, the LUMO of Alq_3 arises only from the π orbital on the quinolate ligand.

SPSTM images are shown in Figure 1a for Alq_3 and Figure 1c for Crq_3. Sub-monolayer coverages show isolated single molecules as bright protrusions with uniform height and size in topography. Differential conductance (dI/dV) is mapped simultaneously with topography to show the alternating magnetization directions on adjacent Cr(001) terraces at a sample bias of -0.4V (Figure 1b and 1d). This is a crucial internal control that establishes spin polarization of the tunneling current during all experiments reported here. The terrace with higher conductance is referred to as "parallel" (P) since its local magnetization is predominantly in the same direction as that of the probe tip. The terrace with lower conductance is similarly referred to as "antiparallel" (AP) since its local magnetization is predominantly opposite to that of the tip. By comparing tunneling spectra measured on adjacent terraces and computing the normalized spin asymmetry, a measure of the spin-polarized density of states is obtained.[34] The molecular features in differential conductance maps also appear as simple bright protrusions with no sub-molecular spatial contrast in our measurements. We note

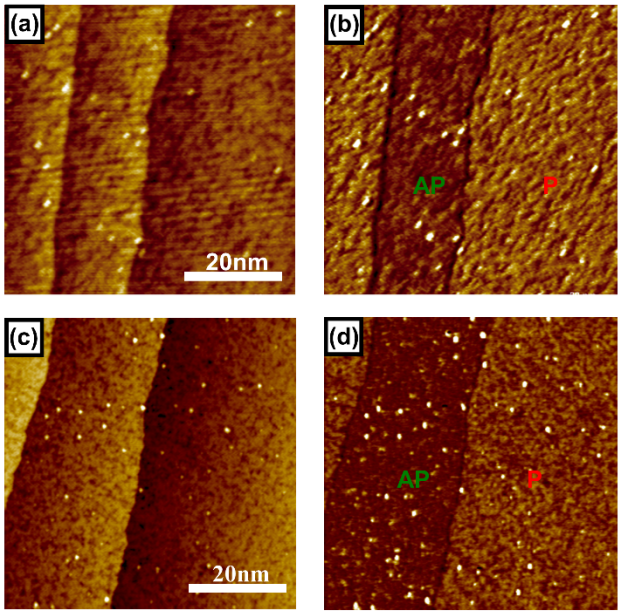

Figure 1 (a) Spin polarized topography of Alq_3/Cr(001) (43 nm x 43 nm, I = 1 nA, U = -0.4 V); **(b)** Conductance map measured simultaneously with the topography in (a); Alq_3/Cr(001) **(c)** 50nm×50nm topographic STM image of submonolayer Crq_3 measured at I=1 nA, U=-0.4V and; **(d)** corresponding differential conductance map.

that conductance maps are measured in constant current mode simultaneously with topography so that there is some topographic convolution.

SP-STS measurements on the exposed Cr(001) surface are shown in Figure 2a, and show the well-known d_z^2-like surface state located near the Fermi level.[40] Spectra on parallel (red) and antiparallel (green) terraces show spin asymmetry in this state, which provides an ideal model system for understanding molecule-surface interactions in organic spintronic device materials. A Lorentzian fit to the surface state peak gives its energy position at 18±3 meV, and we find a spin asymmetry (Figure 2b) for this component of ~ 2 to 10 %, depending upon tip polarization.[34]

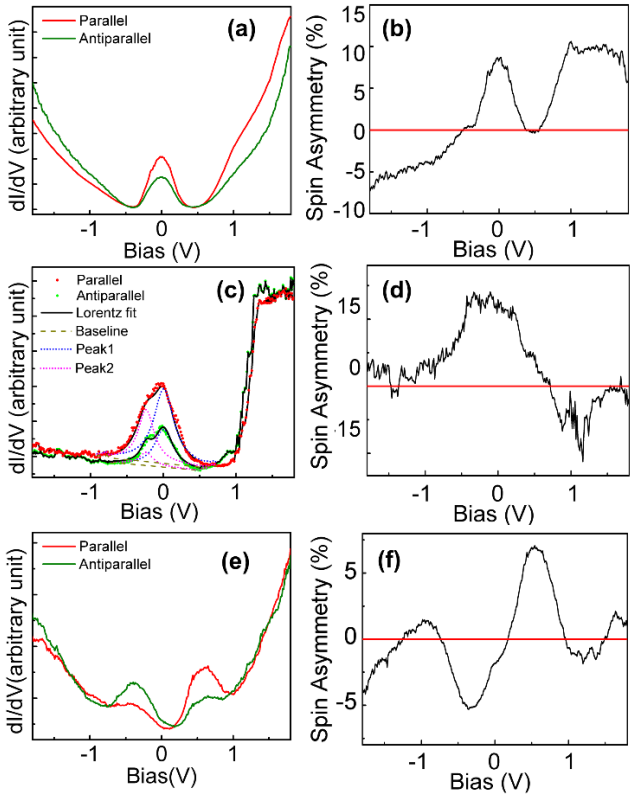

Figure 2 (a) dI/dV spectra measured for the Cr(001) surface on parallel (red line) terraces and antiparallel (green line) terraces (I=700pA, U=-0.6V). Each spectrum shown here is an average of 30 point spectra; **(c)** Spin polarized dI/dV spectra measured on Alq_3 molecules and; **(e)** Crq_3 molecules; Right panels **(b), (d), (f)** show the spin asymmetry calculated from the corresponding dI/dV curves to the left.

Figure 2c shows SP-STS measurements averaged over different Alq_3 adsorbates to check for reproducibility. No variations between different adsorbates were observed in our experiments. We see immediately that Alq_3 significantly changes the spin asymmetry near the Fermi level compared to the bare substrate. An asymmetric spin polarized feature centered near the Fermi level is observed that is similar to the adsorbate-induced changes some of us recently reported for

PTCDA on Cr(001) (see also Supplemental Figure S2).[41] We follow this work in assigning and fitting the asymmetric feature as the result of two overlapping states: the d_z^2 surface state of Cr(001) and an interface state induced by the Alq_3 molecule (a good electron acceptor) created by charge transfer from the Cr substrate. Peak 1 (blue dotted line) is located at 16±2 meV, essentially the same as the surface state of Cr(001), and is broadened by indirect interactions with the substrate. Similar to the case of PTCDA on Cr(001),[41] his broadening is dependent on distance from the molecule as shown in Supplemental Figure S2.[33, 42] An additional peak (orange dotted line) is centered at -240±26 meV. The detailed nature of interface state overlapping the Fermi level will be discussed using the DFT calculations presented below. This indirect interaction mechanism defines a metallic interfacial spin filter since the interface state overlaps the Fermi level and significantly enhances the net spin asymmetry (Figure 2d) compared to the bare Cr(001) surface (Figure 2b).

A startling contrast in spin dependent electronic structure is seen in SP-STS measurements for Crq_3 molecules adsorbed on Cr(001). At the Crq_3 adsorption sites, the original Cr(001) surface state is *not* observed. Instead, Figure 2e shows two new spin-polarized states located at -0.4 eV and +0.6 eV that exhibit opposite signs of spin asymmetry (Figure 2f). These spin-polarized states are immediately reminiscent of bonding and antibonding states formed by hybridization of Crq_3 orbitals with the d_z^2 surface state. The gap separating these states defines a *resistive* spin filter at the Crq_3-Cr interface in

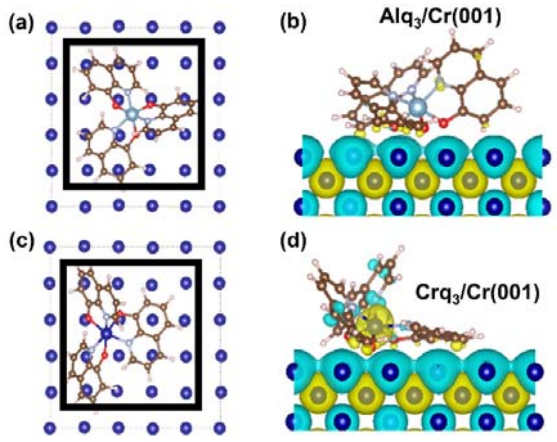

Figure 3 a, c, top view of the Cr(001) surface upon the adsorption of Alq_3 (**a**) and Crq_3 (**c**) molecules, respectively. The dashed squares indicate the unit cell and the solid squares highlight the surface atoms used for PDOS analysis. **b, d**, side view of Alq_3 (**b**) and Crq_3 (**d**) single molecules adsorbed on Cr(001) surface. Both molecules are significantly bent due to interaction with substrate. The blue and yellow color indicate spin distribution of Crq_3/Cr(001) and Alq_3/Cr(001) systems.

contrast to the metallic filter at the Alq_3/Cr(001) interface.

Microscopic insights about the Alq_3/Cr(001) and Crq_3/Cr(001) interfaces have been obtained by first-principles DFT calculations[43, 44] illustrated in Figure 3 (see Supplemental Materials[33]). From side views, one can see that both Crq_3 (Figure 3b) and Alq_3 (Figure 3d) are distorted when adsorbed on Cr(001), indicating strong interactions with the substrate. The total binding energy is 9.35 eV for Crq_3/Cr(001) and 7.72 eV for Alq_3/Cr(001). This difference immediately points to the differences in interactions between the two adsorbates. Moreover, the adsorption geometry seen in Figure 3 for each molecule is different, with Crq_3 maintaining ligand π planes more parallel to the surface than for Alq_3. In addition, the Cr(III)-Cr vertical distance is shorter than the Al(III)-Cr distance.

The adsorption configurations observed in our DFT study are interesting to compare with Alq_3 on Cobalt surfaces.[45] For both Alq_3 and Crq_3 on the Cr(001) surface we find larger molecular distortions compared to the free molecule geometry and larger total binding energies than for any of the adsorption geometries of Alq_3 on Cobalt. The comparison illustrates why we find experimental evidence for only one adsorbed species in our SP-STS measurements. Specifically, such strong interactions establish a single preferred adsorption structure with little possibility of competition from other structures.

The spin distribution in both interface systems is resolved in the side views (Figure 3b and 3d) and shows spin polarization at the metal-organic interface. Our calculations predict an antiparallel arrangement of in-plane spin density on the outer substrate layer and both of the molecular adsorbates as indicated by the blue-to-yellow color scale in Figure 3. The local magnetic moments are notably reduced from ~ 2.7 μ_B on the metal to ~ 1.2 μ_B beneath the Alq_3 adsorbate or ~1.1 μ_B beneath Crq_3 (see Supplemental Figure S3[33]), similar to the effect seen in DFT calculations for C_{60} on Cr(001).[25] We note that the difference in adsorbate modification of

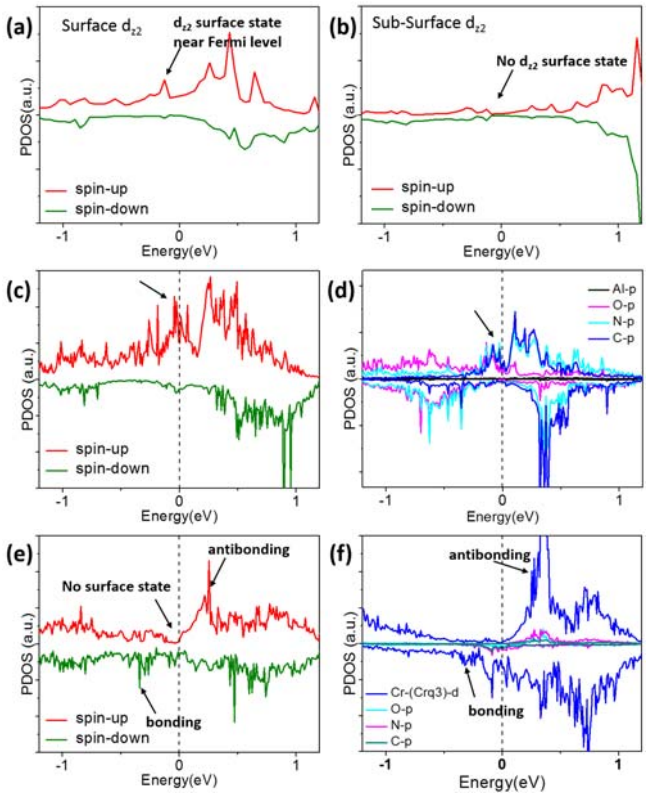

Figure 4 Projected density of states from DFT calculations; (**a**)Surface atoms of the Cr(001) substrate with no adsorbates; **(b)** Bulk atoms in the interior of the Cr(001) slab; **(c)** Cr surface atoms in the Alq_3/Cr(001) system, where a peak remains near the Fermi level (marked by arrow); **(d)** An extra peak (marked by arrow) just below Fermi level is illustrated for the Alq_3 adsorbate *p* orbitals on a C, O, and N atoms and overlaps the surface state region from (c); **(e)** In the Crq_3/Cr(001) system, the surface state of Cr(001) is not present due to hybridization with molecule and is replaced by two new peaks separated by a gap labelled as bonding and antibonding; **(f)** The two new peaks also have significant weight and spin asymmetry in PDOS on the d_z^2 orbital of the Crq_3 adsorbate.

local magnetic moment for Alq_3 compared to Crq_3 agrees with the general picture of a more significant adsorbate interaction in the latter case. Due to the strength of interaction and the detailed electronic structure considerations discussed below, we assign the origin of this antiparallel orientation to be *direct exchange* between substrate spins and the electrons in the molecule. We note that this contrasts with the superexchange interactions predicted for Feq_3 on a cobalt substrate.[46]

The detailed electronic and magnetic impact of adsorption differences between Crq_3 and Alq_3 can be seen in the spin-resolved Projected Density of States (PDOS) in Figure 4 inside the regions marked with black squares in Figure 3a,c. Figure 4a and 4b show the pristine Cr(001) substrate PDOS for the surface and interior of the slab respectively, where the low energy surface state is clearly seen in Figure 4a. The PDOS for substrate atoms underneath an Alq_3 adsorbate shown in Figure 4c still exhibits a broadened peak near the Fermi

level. The peak is also present in the PDOS on the molecule in Alq_3 shown in Figure 4d, which is dominated by *p* orbitals on ligand atoms. The interface state enhances spin asymmetry in the PDOS as in our experimental data, and has significant spatial localization on ligand N atoms similar to what has also been found in element-specific XMCD studies of Alq_3 on cobalt.[30] The spin asymmetry located on the molecule has the same sign as the Cr surface state in agreement with SP-STS observations.

In contrast, the PDOS for Cr substrate atoms beneath Crq_3 molecules (Figure 4e and 4f) exhibits *no* spin-polarized surface state exactly as observed in the experiment. Instead, new enhancements in PDOS located both above and below the original surface state position are seen as indicated by the arrows. These can be viewed as arising from the hybridization of the surface state with the Crq_3 LUMO. The spin polarization for the peak above the Fermi level is of the same sign as the surface state while the peak below the Fermi level has the opposite sign of spin polarization. This agrees with the reversal of spin asymmetry above and below the Fermi level in the experimental asymmetry in Figure 2f.

Figure 4f shows that the PDOS on a Crq_3 molecule adsorbed on Cr(001) exhibits similar bonding and antibonding peaks as the substrate, as expected for states that are admixtures of both substrate and molecular orbital states. Moreover, the hybridized states are mainly localized on the Cr(III) center on molecule, indicating that the d_z^2 contributors to the Crq_3 LUMO are mostly responsible for the strong direct coupling to substrate surface state.

The significance of the comparison of Crq_3 and Alq_3 is in the implications for the extreme sensitivity of magnetic interface states to molecular orbital details. Remarkably, this leads to variations between the extreme cases of resistive or metallic spin filters with only minor molecular changes.[4] Such a striking difference is not obvious from a comparison on the molecular orbitals of the molecules viewed in isolation (e.g. see Supplemental Figure S1c and S1d).[33] Both Alq_3 and Crq_3 interact strongly with the Cr substrate and have very similar frontier

molecule orbitals. It only takes a subtle change in the *d*-orbital content in the LUMO of Crq_3 compared to Alq_3 to qualitatively change the character of the interface state from metallic to resistive.

In the case of Crq_3, the interfacial interaction is covalent in nature with bonding and antibonding interface states that create a resistive interface. This is precisely the strong coupling regime in the famous Anderson-Newns-Grimely model[47-49] of chemisorption sometimes referred to as the "magnetic" regime. Our observations directly connect with this regime by demonstrating the reversal of spin asymmetry for the two new interface states. Importantly, while it may be difficult to predict when interactions will be strong enough to obtain the magnetic regime, it is clear that this is a useful design strategy for creating a resistive spin filter. This type of interface might be more effective for direct spin injection into thick organic transport layers as opposed to TMR-based devices. This type of resistive filter is also of interest given new observations of dynamic spin filtering effects near metal organic interfaces.[32]

By contrast the charge-transfer type interaction for Alq_3 leaves spin polarized states at the Fermi level that in turn establish a metallic interface. A metallic interface would likely be advantageous for applications of traditional organic TMR devices[3, 27] where states at the electrode Fermi level control conductance. Indeed, this type of spin filtering is required to explain the 300% TMR in Alq_3 nanopores[3], and our model interface is the direct proof that enhancement of interface polarization at a magnetic electrode can result from a single Alq_3 molecule. Thus, our observations and calculations presented here provide a specific microscopic mechanism for spin filtering at Alq_3 –metal interfaces through charge transfer interactions. The giant TMR effects seen in nanopores are much larger than the spin asymmetries seen here but the qualitative origin of the interactions is relevant.

Spin-dependent electronic interactions at interfaces need to be carefully tuned *even within the very strong interaction regime* to reliably control spin filter mechanisms. We can see a diverse

range of strong spin dependent interfacial coupling mechanisms with each having distinct practical consequences for spin injection. The sensitivity of hybrid interface states at electrodes to small molecule changes is a clear opportunity for interfacial design in both organic spintronics and semiconductor spintronics more broadly. This work was supported by the U.S. Department of Energy, Office of Science, Basic Energy Sciences under award No. DE-SC0010324. The computation work at Utah was supported by NSF-MRSEC (Grand No. DMR-1121252) (WJ) and U.S. DOE-BES (Grant No. DE-FG02-04ER46148) (FL).

References

1. V. A. Dediu, L. E. Hueso, I. Bergenti and C. Taliani, Nature materials **8** (9), 707-716 (2009).
2. S. Sanvito, Nature Physics **6** (8), 562-564 (2010).
3. C. Barraud, P. Seneor, R. Mattana, S. Fusil, K. Bouzehouane, C. Deranlot, P. Graziosi, L. Hueso, I. Bergenti and V. Dediu, Nature Physics **6** (8), 615-620 (2010).
4. K. V. Raman, Applied Physics Reviews **1** (3), 031101 (2014).
5. Y. Q. Zhan and M. Fahlman, Journal of Polymer Science Part B-Polymer Physics **50** (21), 1453-1462 (2012).
6. G. Schmidt, Journal of Physics D-Applied Physics **38** (7), R107-R122 (2005).
7. R. Jansen, S. P. Dash, S. Sharma and B. C. Min, Semiconductor Science and Technology **27** (8), 083001 (2012).
8. I. Appelbaum, B. Q. Huang and D. J. Monsma, Nature **447** (7142), 295-298 (2007).
9. M. Cinchetti, V. A. Dediu and L. E. Hueso, Nat Mater **16** (5), 507-515 (2017).
10. J. S. Moodera, T. S. Santos and T. Nagahama, Journal of Physics-Condensed Matter **19** (16), 165202 (2007).
11. W. H. Butler, Science and Technology of Advanced Materials **9** (1), 014106 (2008).
12. A. Riminucci, M. Prezioso, C. Pernechele, P. Graziosi, I. Bergenti, R. Cecchini, M. Calbucci, M. Solzi and V. A. Dediu, Applied Physics Letters **102** (9) (2013).
13. Z. G. Yu, Physical Review Letters **111** (1) (2013).
14. J. Brede and R. Wiesendanger, Physical Review B **86** (18) (2012).
15. C. H. Hsu, Y. H. Chu, C. I. Lu, P. J. Hsu, S. W. Chen, W. J. Hsueh, C. C. Kaun and M. T. Lin, Journal of Physical Chemistry C **119** (6), 3374-3378 (2015).

16. S. Lach, A. Altenhof, K. Tarafder, F. Schmitt, M. E. Ali, M. Vogel, J. Sauther, P. M. Oppeneer and C. Ziegler, Advanced Functional Materials **22** (5), 989-997 (2012).
17. S. Schmaus, A. Bagrets, Y. Nahas, T. K. Yamada, A. Bork, M. Bowen, E. Beaurepaire, F. Evers and W. Wulfhekel, Nature nanotechnology **6** (3), 185-189 (2011).
18. N. Atodiresei, J. Brede, P. Lazić, V. Caciuc, G. Hoffmann, R. Wiesendanger and S. Blügel, Physical review letters **105** (6), 066601 (2010).
19. C. Iacovita, M. V. Rastei, B. W. Heinrich, T. Brumme, J. Kortus, L. Limot and J. P. Bucher, Physical Review Letters **101** (11), 116602 (2008).
20. T. Methfessel, S. Steil, N. Baadji, N. Grossmann, K. Koffler, S. Sanvito, M. Aeschlimann, M. Cinchetti and H. J. Elmers, Physical Review B **84** (22), 224403 (2011).
21. J. Schwobel, Y. S. Fu, J. Brede, A. Dilullo, G. Hoffmann, S. Klyatskaya, M. Ruben and R. Wiesendanger, Nature Communications **3**, 953 (2012).
22. S. Gueddida, M. Gruber, T. Miyamachi, E. Beaurepaire, W. Wulfhekel and M. Alouani, Journal of Physical Chemistry Letters **7** (5), 900-904 (2016).
23. Y. H. Chu, C. H. Hsu, C. I. Lu, H. H. Yang, T. H. Yang, C. H. Luo, K. J. Yang, S. H. Hsu, G. Hoffmann, C. C. Kaun and M. T. Lin, Acs Nano **9** (7), 7027-7032 (2015).
24. K. V. Raman, A. M. Kamerbeek, A. Mukherjee, N. Atodiresei, T. K. Sen, P. Lazic, V. Caciuc, R. Michel, D. Stalke, S. K. Mandal, S. Blugel, M. Munzenberg and J. S. Moodera, Nature **493** (7433), 509-513 (2013).
25. S. Kawahara, J. Lagoute, V. Repain, C. Chacon, Y. Girard, S. Rousset, A. Smogunov and C. Barreteau, Nano letters **12** (9), 4558-4563 (2012).
26. Z. Xiong, D. Wu, Z. V. Vardeny and J. Shi, Nature **427** (6977), 821-824 (2004).
27. T. Santos, J. Lee, P. Migdal, I. Lekshmi, B. Satpati and J. Moodera, Physical review letters **98** (1), 016601 (2007).
28. D. Sun, L. Yin, C. Sun, H. Guo, Z. Gai, X.-G. Zhang, T. Z. Ward, Z. Cheng and J. Shen, Physical review letters **104** (23), 236602 (2010).
29. V. Dediu, L. Hueso, I. Bergenti, A. Riminucci, F. Borgatti, P. Graziosi, C. Newby, F. Casoli, M. De Jong and C. Taliani, Physical Review B **78** (11), 115203 (2008).
30. Y. Zhan, E. Holmström, R. Lizárraga, O. Eriksson, X. Liu, F. Li, E. Carlegrim, S. Stafström and M. Fahlman, Advanced Materials **22** (14), 1626-1630 (2010).
31. S. Steil, N. Grossmann, M. Laux, A. Ruffing, D. Steil, M. Wiesenmayer, S. Mathias, O. L. A. Monti, M. Cinchetti and M. Aeschlimann, Nature Physics **9** (4), 242-247 (2013).
32. A. Droghetti, P. Thielen, I. Rungger, N. Haag, N. Groszmann, J. Stockl, B. Stadtmuller, M. Aeschlimann, S. Sanvito and M. Cinchetti, Nat Commun **7** (2016).
33. (See Supplemental Material at).
34. R. Wiesendanger, Reviews of Modern Physics **81** (4), 1495 (2009).
35. D. Evans, Journal of the Chemical Society, 2003-2005 (1959).
36. L. M. Monzon, F. Burke and J. Coey, The Journal of Physical Chemistry C **115** (18), 9182-9192 (2011).
37. A. Schlenhoff, S. Krause, G. Herzog and R. Wiesendanger, Applied Physics Letters **97** (8), 083104 (2010).
38. A. R. Freitas, M. Silva, M. L. Ramos, L. L. Justino, S. M. Fonseca, M. M. Barsan, C. M. Brett, M. R. Silva and H. D. Burrows, Dalton Transactions **44** (25), 11491-11503 (2015).
39. M. Mason, C. Tang, L. Hung, P. Raychaudhuri, J. Madathil, D. Giesen, L. Yan, Q. Le, Y. Gao and S. Lee, Journal of Applied Physics **89** (5), 2756-2765 (2001).
40. M. Kleiber, M. Bode, R. Ravlić, N. Tezuka and R. Wiesendanger, Journal of magnetism and magnetic materials **240** (1), 64-69 (2002).
41. J. Wang and D. B. Dougherty, Physical Review B **92** (16), 161401 (2015).

42. S. Zhang, P. Levy and A. Fert, Physical Review B **45** (15), 8689 (1992).
43. G. Kresse and D. Joubert, Physical Review B **59** (3), 1758 (1999).
44. J. P. Perdew and W. Yue, Physical review B **33** (12), 8800 (1986).
45. Y.-P. Wang, X.-F. Han, Y.-N. Wu and H.-P. Cheng, Physical Review B **85** (14), 144430 (2012).
46. W. Jiang, M. Zhou, Z. Liu, D. Sun, Z. Vardeny and F. Liu, Journal of Physics: Condensed Matter **28** (17), 176004 (2016).
47. D. M. Newns, Physical Review **178** (3), 1123-1135 (1969).
48. J. K. Norskov, Reports on Progress in Physics **53** (10), 1253 (1990).
49. P. W. Anderson, Physical Review **124** (1), 41-53 (1961).

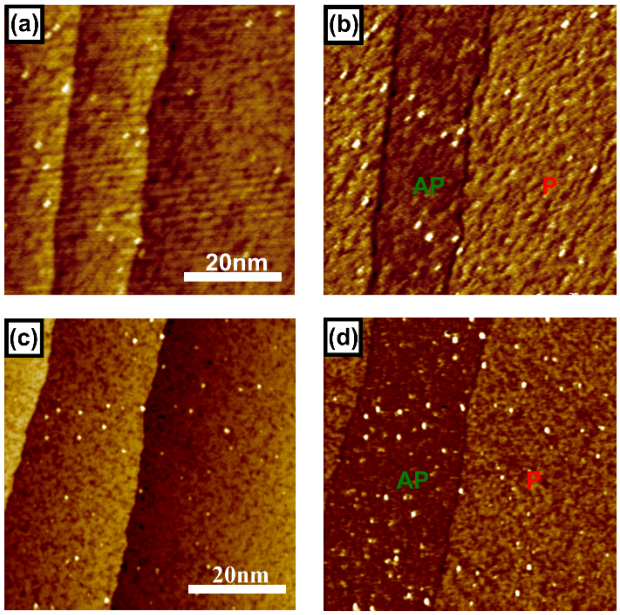

Figure 1 (a) Spin polarized topography of Alq_3/Cr(001) (43 nm x 43 nm, I = 1 nA, U = -0.4 V); **(b)** Conductance map measured simultaneously with the topography in (a); Alq_3/Cr(001) **(c)** 50nm×50nm topographic STM image of submonolayer Crq_3 measured at I=1 nA, U=-0.4V and; **(d)** corresponding differential conductance map.

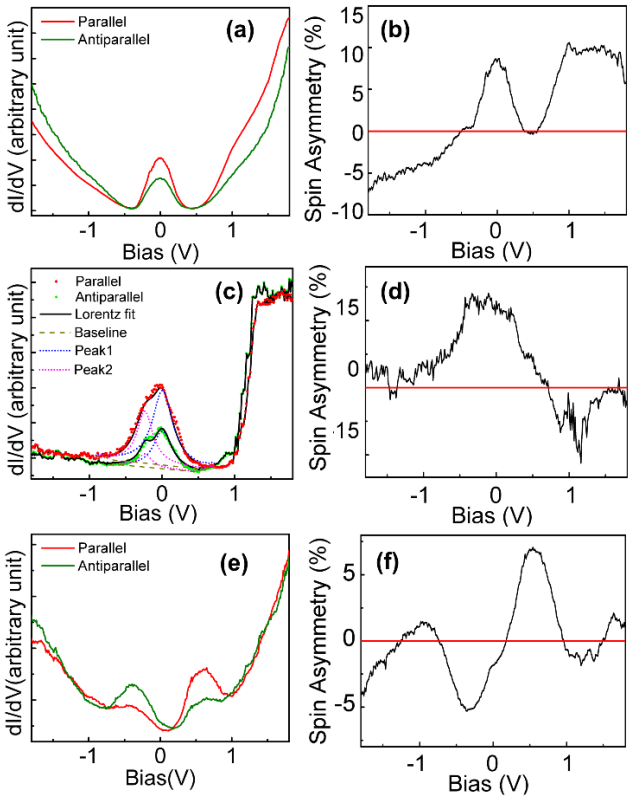

Figure 2 (a)) dI/dV spectra measured for the Cr(001) surface on parallel (red line) terraces and antiparallel (green line) terraces (I=700pA, U=-0.6V). Each spectrum shown here is an average of 30 point spectra; **(c)** Spin polarized dI/dV spectra measured on Alq_3 molecules and; **(e)** Crq_3 molecules; Right panels **(b), (d), (f)** show the spin asymmetry calculated from the corresponding dI/dV curves to the left.

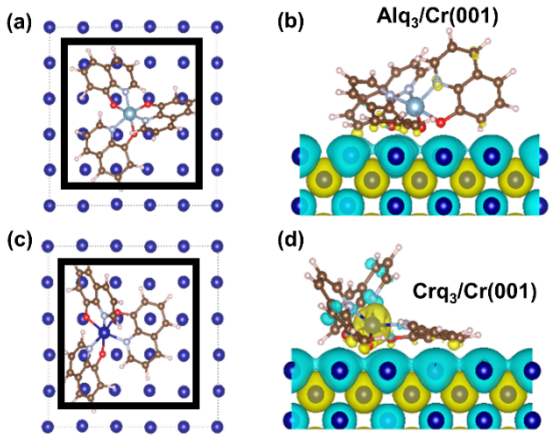

Figure 3 a, c, top view of the Cr(001) surface upon the adsorption of Alq_3 (**a**) and Crq_3 (**c**) molecules, respectively. The dashed squares indicate the unit cell and the solid squares highlight the surface atoms used for PDOS analysis. **b, d**, side view of Alq3 (**b**) and Crq_3 (**d**) single molecules adsorbed on Cr(001) surface. Both molecules are significantly bent due to interaction with substrate. The blue and yellow color indicate spin distribution of Crq_3/Cr(001) and Alq_3/Cr(001) systems.

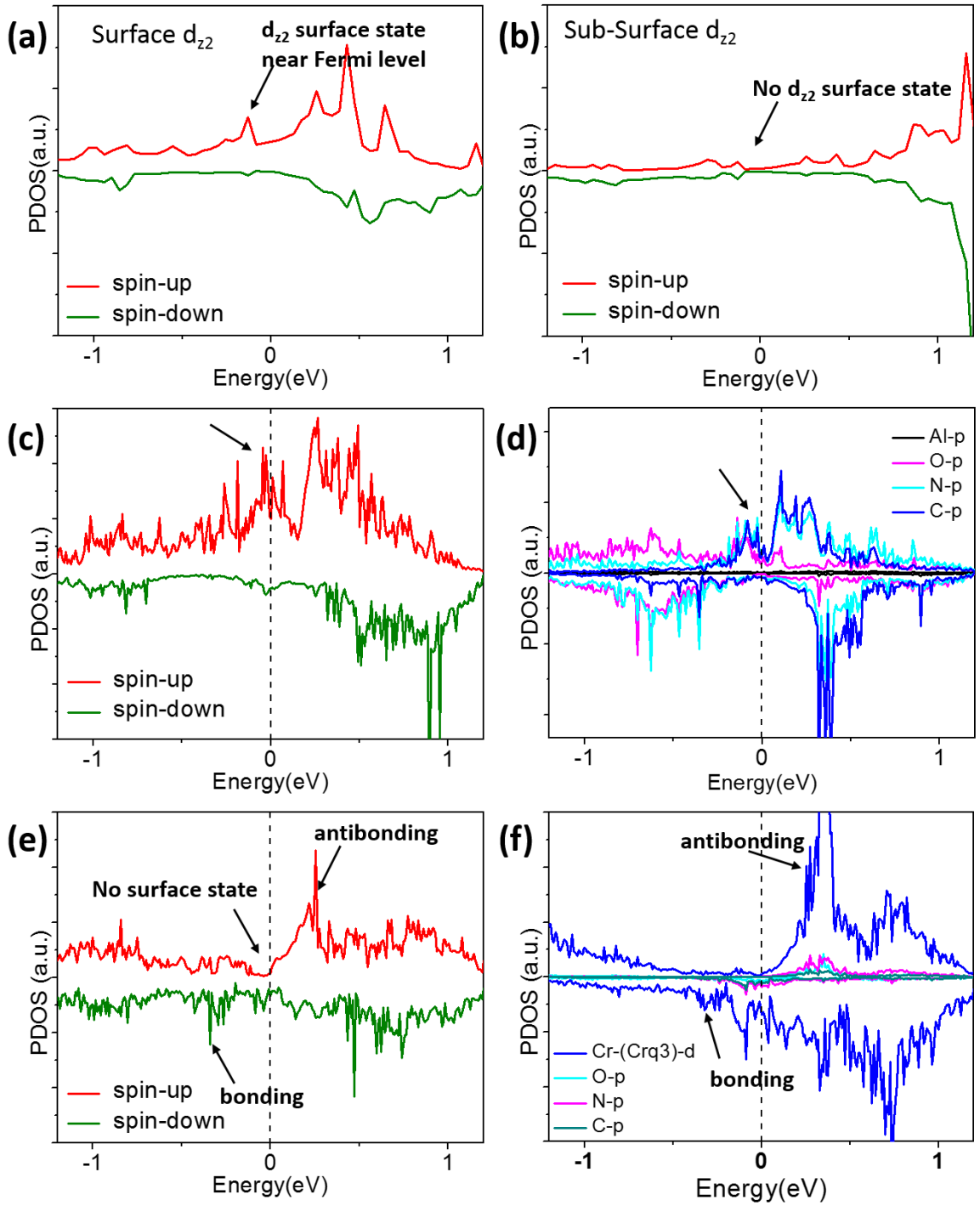

Figure 4 Projected density of states from DFT calculations; (**a**)Surface atoms of the Cr(001) substrate with no adsorbates; **(b)** Bulk atoms in the interior of the Cr(001) slab; **(c)** Cr surface atoms in the Alq_3/Cr(001) system, where a peak remains near the Fermi level; **(d)** An extra peak just below Fermi level is illustrated for the Alq_3 adsorbate *p* orbitals on a C, O, and N atoms and overlaps the surface state region from (c); **(e)** In the Crq_3/Cr(001) system, the surface state of Cr(001) is not present due to hybridization with molecule and is replaced by two new peaks

separated by a gap labelled as bonding and antibonding; **(f)** The two new peaks also have significant weight and spin asymmetry in PDOS on the d_z^2 orbital of the Crq_3 adsorbate.